Hyperfine-dependent lifetimes in Be-like ions

M. Andersson, Y. Zou, and R. Hutton*
The Key Laboratory of Applied Ion Beam Physics, Ministry of Education, People's Republic of China and Shanghai EBIT Laboratory, Institute of Modern Physics, Fudan University, Shanghai, People's Republic of China

T. Brage
Department of Physics, Lund University, Sweden
(Received 15 December 2008; published 3 March 2009)

Theoretical investigations of hyperfine quenching of the two metastable levels $1s^2 2s2p\ ^3P_0$ and $^3P_2$ have been performed along the Be-like isoelectronic sequence for ions between $Z=6-22$. It is shown that the lifetime of the latter level is sensitive to hyperfine quenching in the beginning of the isoelectronic sequence, but the sensitivity decreases towards the high-Z end. It is also shown that the hyperfine dependent branching fraction between the $2s^2\ ^1S_0-2s2p\ ^3P_2$ and the $2s2p\ ^3P_1-2s2p\ ^3P_2$ transitions can lead to some rather drastic changes in the spectra. Our predicted value of 0.677 s^{-1} for the hyperfine-induced $2s^2\ ^1S_0-2s2p\ ^3P_0$ transition rate for $^{47}Ti^{18+}$ are in disagreement with a recent experimental value of 0.56(3) s^{-1}. Our calculated values of this quenching are in agreement with other recent calculations all along the sequence.

DOI: 10.1103/PhysRevA.79.032501 PACS number(s): 31.10.+z, 31.15.A−, 32.10.Fn, 32.70.Cs

I. INTRODUCTION

As part of our ongoing investigations of what could be considered as the third generation of forbidden lines, a theoretical investigation of hyperfine quenching of the two metastable levels $2s2p\ ^3P_0$ and $^3P_2$ in Be-like ions has been performed. To the best of our knowledge hyperfine quenching of the $^3P_2$ level has not previously been studied, whereas the $^3P_0$ level has been the subject of several investigations.

$2s2p\ ^3P_0$ is the first excited level in Be-like ions and in the absence of a nuclear spin it has no allowed single photon decay channels to the $2s^2\ ^1S_0$ ground state, but can only decay through the extremely slow two-photon process. In the presence of a finite nuclear spin the off-diagonal hyperfine interaction introduce a mixing between $2s2p\ ^3P_0$ and $2s2p\ ^3P_1$ and $^1P_1$, respectively, opening a hyperfine induced electric dipole transition to the ground state. Theoretical investigations of this hyperfine quenching have been performed on several occasions. Marques *et al.* [1] performed an investigation along the whole isoelectronic sequence using multiconfiguration Dirac-Hartree-Fock (MCDHF) calculations and the complex matrix scheme. In these calculations only the hyperfine mixing with the $2s2p\ ^3P_1$ state was taken into consideration. Brage *et al.* [2] used the multiconfiguration Hartree-Fock (MCHF), the MCDHF, and F-dependent configuration interaction (FCI) method in a later investigation of a few, mainly low Z, ions. In that work it was shown that the hyperfine mixing with the $2s2p\ ^1P_1$ state was of great importance at least in the beginning of the isoelectronic sequence. In a recent paper by Cheng *et al.* [3] ions along the whole Be-like isoelectronic sequence were investigated using a relativistic configuration interaction method. In that work quenching induced by mixing with both the $^3P_1$ and the $^1P_1$ levels was calculated using both a perturbative and a radiation damping approach.

On the experimental side, very few measurements of hyperfine-induced decay rates are available. Schippers *et al.* [4] measured the $2s^2\ ^1S_0-2s2p\ ^3P_0$ transition rate for $^{47}Ti^{18+}$ to be 0.56(3) s^{-1}. This value is in disagreement with the predicted value of 0.6727 s^{-1} by Cheng *et al.* [3]. From observations of the planetary nebula NGC3918, Brage *et al.* [5] experimentally determined the hyperfine-induced decay rate for an admixture of $^{14}N^{3+}$ and $^{15}N^{3+}$ to be $4\times10^{-4}\pm33\%$ s^{-1} in agreement with the predicted rate of 4.92×10^{-4} and 3.62×10^{-4} for the two isotopes, respectively, by Brage *et al.* [2] and 4.440×10^{-4} and 3.269×10^{-4} by Cheng *et al.* [3]. Unfortunately, the uncertainties in the measurement reported in [5] are not good enough to rule out a similar disagreement as found by Schippers *et al.* [4].

Hyperfine quenching of metastable levels which have competing one-photon decay channels has attracted some attention in recent years. Yao *et al.* [6,7] investigated the lifetime of the first excited level, $3d^9 4s\ ^3D_3$, in Ni-like xenon, explaining the earlier discrepancies between theoretical predictions and an experimentally determined lifetime by Träbert *et al.* [8]. Following this paper Träbert *et al.* [9] measured the lifetime of isotopically pure ^{129}Xe and ^{132}Xe, where the former isotope has a nuclear spin $I=1/2$ and the latter no nuclear spin. These measurements confirmed the predictions by Yao *et al.* [6,7]. In a later theoretical work Andersson *et al.* [10] investigated the importance of hyperfine quenching along the Ni-like isoelectronic sequence.

Some work has also been performed concerning hyperfine quenching of levels of the type $nsnp\ ^3P_2$ in systems homologous to Be-like ions. The $^3P_2$ level is the third excited state in all of these systems and in the absence of a nuclear spin, it decays mainly through two different transition channels, a magnetic quadrupole transition to the ground state and a magnetic dipole transition to the $nsnp\ ^3P_1$ level. Already in the 1960s, Garstang [11,12] investigated the hyperfine quenching of these levels in neutral magnesium, zinc, and cadmium. The aim was to determine whether the

*rhutton@fudan.edu.cn

$ns^2\ ^1S_0$–$nsnp\ ^3P_2$ lines, seen in the corresponding spectra, are dominated by the hyperfine-induced electric dipole or the magnetic quadrupole transition channel. Porsev and Derevianko [13] investigated the same type of hyperfine quenching in neutral magnesium, calcium, strontium, and ytterbium in connection with the aim of designing an ultraprecise optical clock. In a recent paper, Andersson *et al.* [14] investigated the hyperfine quenching of the $4s4p\ ^3P_2$ level in the Zn-like isoelectronic sequence. It was shown that hyperfine quenching has a large impact on the lifetime of $^3P_2$ for low-Z members of the sequence, but its influence decreases fairly quickly with increasing Z.

II. THEORY

A. Hyperfine interaction

In an isotope with a nuclear spin **I**, the nucleus has electromagnetic multipole moments which interacts with different aspects of the fields generated by the electrons. This interaction splits each fine-structure level into multiple hyperfine levels leading to a coupling of the total electronic angular momentum **J** and the nuclear spin **I** to a new total angular momentum **F**, defining the hyperfine levels. Since the hyperfine interaction operator $\mathcal{H}_{hpf}$ does not commute with **J**, the off-diagonal hyperfine interaction introduce mixing between levels with different J quantum numbers opening up new transition channels.

In this work, both the nuclear magnetic dipole and electric quadrupole hyperfine interaction were included. The hyperfine interaction operator could then be expressed as

$$\mathcal{H}_{hpf} = \boldsymbol{T}^{(1)} \cdot \boldsymbol{M}^{(1)} + \boldsymbol{T}^{(2)} \cdot \boldsymbol{M}^{(2)}. \tag{1}$$

$\mathbf{T}^{(k)}$ and $\mathbf{M}^{(k)}$ are spherical tensors of rank k where the former operates on the electronic part of the wave function and the latter on the nuclear part. $k=1$ represents the nuclear magnetic dipole and $k=2$ the nuclear electric quadrupole hyperfine interaction. The hyperfine interaction matrix element between two hyperfine levels $|\gamma IJFM_F\rangle$ and $|\gamma' IJ'FM_F\rangle$ then consists of two parts,

$$\langle \gamma IJFM_F|\mathcal{H}_{hpf}|\gamma' IJ'FM_F\rangle = W_{M1}(J,J') + W_{E2}(J,J'), \tag{2}$$

where W_{M1} represents the nuclear magnetic dipole hyperfine interaction and W_{E2} the nuclear electric quadrupole hyperfine interaction. Using the Brink and Satchler definition of the reduced matrix element [15], the two types of interaction can be calculated from

$$W_{M1}(J,J') = (-1)^{I+J+F}\sqrt{(2J+1)(2I+1)}\begin{Bmatrix} I & J & F \\ J' & I & 1 \end{Bmatrix} \times \langle \gamma J\|\boldsymbol{T}^{(1)}\|\gamma' J'\rangle\langle I\|\boldsymbol{M}^{(1)}\|I\rangle \tag{3}$$

and

$$W_{E2}(J,J') = (-1)^{I+J+F}\sqrt{(2J+1)(2I+1)}\begin{Bmatrix} I & J & F \\ J' & I & 2 \end{Bmatrix} \times \langle \gamma J\|\boldsymbol{T}^{(2)}\|\gamma' J'\rangle\langle I\|\boldsymbol{M}^{(2)}\|I\rangle. \tag{4}$$

The reduced nuclear matrix elements were not calculated using nuclear wave functions, instead we used the conventional definition of the nuclear magnetic dipole moment, μ_I, and the electric quadrupole moment, Q,

$$\langle I\|\boldsymbol{M}^{(1)}\|I\rangle = \mu_I\sqrt{\frac{I+1}{I}}, \tag{5}$$

$$\langle I\|\boldsymbol{M}^{(2)}\|I\rangle = \frac{1}{2}Q. \tag{6}$$

In this work, values of μ_I and Q tabulated by Kurucz [16] were used.

We were interested in the hyperfine mixing between $2s2p\ ^3P_{0,2}$ and $2s2p\ ^3P_1$ and $^1P_1$, respectively. By replacing the reduced nuclear matrix element in Eq. (3) by Eq. (5) and evaluating the 6J symbol, the nuclear magnetic dipole part of the off-diagonal hyperfine interactions could be expressed as

$$W_{M1}(J,J-1) = \frac{\mu_I}{2I}\frac{1}{\sqrt{J(2J-1)}}[(K-2J+1)]^{1/2} \times [(K+1)(K-2F)(K-2I)]^{1/2} \times \langle \gamma J\|\mathbf{T}^{(1)}\|\gamma'(J-1)\rangle, \tag{7}$$

where

$$K = F + J + I. \tag{8}$$

Introducing the off-diagonal nuclear magnetic dipole hyperfine interaction constant, $A(J,J-1)$, defined as

$$A(J,J-1) = \mu_I\frac{1}{I\sqrt{J(2J-1)}}\langle \gamma J\|\mathbf{T}^{(1)}\|\gamma'(J-1)\rangle \tag{9}$$

in the Brink and Satchler [15] sense, expression (7) can be simplified to

$$W_{M1}(J,J-1) = \frac{A(J,J-1)}{2}[J^2-(I-F)^2]^{1/2} \times [(I+F+1)^2-J^2]^{1/2}. \tag{10}$$

From this it follows that the nuclear magnetic dipole hyperfine interaction between $^xP_1$ and $^3P_0$ is given by

$$W_{M1}(^xP_1,{}^3P_0) = \sqrt{I(I+1)}A(^xP_1,{}^3P_0) \tag{11}$$

and the interaction between $^xP_1$ and $^3P_2$ by

$$W_{M1}(^xP_1,{}^3P_2) = \frac{A(^xP_1,{}^3P_2)}{2}[4-(I-F)^2]^{1/2} \times [(I+F+1)^2-4]^{1/2}, \tag{12}$$

where x refers to the singlet or triplet.

In a similar way, the nuclear electric quadrupole hyperfine interaction between two states differing in J by one can be expressed as

$$W_{E2}(J,J-1) = B(J,J-1)(K-2J+1)^{1/2} \times \frac{[3(K+1)(K-2F)(K-2I)]^{1/2}}{2I(2I-1)J(J-1)}[(F+I+1) \times (F-I)-J^2+1] = B(J,J-1) \times [J^2-(I-F)^2]^{1/2} \times [(I+F+1)^2-J^2]^{1/2}\sqrt{3} \times \frac{[F(F+1)-I(I+1)-J^2+1]}{2I(2I-1)J(J-1)}, \quad (13)$$

where the off-diagonal nuclear electric quadrupole hyperfine interaction constant $B(J,J-1)$ is defined as

$$B(J,J-1) = \frac{Q}{2}\left[\frac{J(J-1)}{(J+1)(2J+3)}\right]^{1/2}\langle \gamma J \| \boldsymbol{T}^{(2)} \| \gamma'(J-1)\rangle. \quad (14)$$

There is no electric quadrupole hyperfine interaction between $^3P_1$ and $^xP_1$ [due to triangle rule of the $6J$ symbol in Eq. (4)], but the interaction between $^3P_2$ and $^xP_1$ is given by

$$W_{E2}(^3P_2,{}^xP_1) = B(^3P_2,{}^xP_1)[4-(I-F)^2]^{1/2} \times [(I+F+1)^2-4]^{1/2}\sqrt{3} \times \frac{[F(F+1)-I(I+1)-3]}{4I(2I-1)}. \quad (15)$$

There are several advantages using the off-diagonal A and B constants for investigating hyperfine quenching. Instead of calculating the reduced off-diagonal hyperfine interaction matrix elements for each of the hyperfine levels, the A and B constants only have to be calculated once and used for all of the hyperfine levels. Another advantage is that there is a simple algebraic expression linking their values for different isotopes. Therefore the hyperfine interaction for one isotope can easily be derived from the value for another, by simple rescaling laws

$$A(\beta) = \frac{\mu_I(\beta)}{I(\beta)}\frac{I(\alpha)}{\mu_I(\alpha)}A(\alpha) \quad (16)$$

and

$$B(\beta) = \frac{Q(\beta)}{Q(\alpha)}B(\alpha). \quad (17)$$

Hyperfine interaction constants were also convenient for investigating the importance of including the nuclear electric quadrupole hyperfine interaction, which has been left out in some earlier calculations.

B. Hyperfine quenching

The transition probability for an electric dipole transition between two hyperfine levels is given by

$$A_{E1}(\gamma IJF,\gamma' IJ'F') = \frac{(2\pi)^3}{3\hbar\lambda^3}\frac{1}{2F'+1} \times |\langle \gamma IJF \| D^{(1)} \| \gamma' IJ'F'\rangle|^2. \quad (18)$$

The reduced matrix elements can in turn be expressed in J-dependent reduced matrix elements as

$$\langle \gamma IJF \| D^{(1)} \| \gamma' IJ'F'\rangle = \sqrt{(2F+1)(2F'+1)} \times (-1)^{J+I+F'+1}\begin{Bmatrix} J & I & F \\ F' & 1 & J' \end{Bmatrix} \times \langle \gamma J \| D^{(1)} \| \gamma' J'\rangle. \quad (19)$$

In this work we were interested in hyperfine transitions to the ground state $2s^2\,{}^1S_0$ which only have one hyperfine level. From an orthogonality relationship for the $6J$ symbols, the transition rate could then be simplified as

$$A_{E1}(\gamma IJF,\gamma' IJ'F') = \frac{(2\pi)^3}{3\hbar\lambda^3}\frac{1}{2J'+1}|\langle \gamma J \| D^{(1)} \| \gamma' J'\rangle|^2, \quad (20)$$

i.e., the same expression as for the transition between the fine-structure levels in the case of an isotope with no nuclear spin. The hyperfine mixing with $2s2p\,{}^3P_1$ and $^1P_1$ opens up a hyperfine-induced electric dipole transition channel to the ground state for both the $2s2p\,{}^3P_0$ and the $^3P_2$ level. The transition rates for these transitions could be calculated using

$$A_{hpf}(^1S_0,{}^3P_yF) = \frac{(2\pi)^3}{3\hbar\lambda^3}\frac{1}{3}|c_{^1P_1}(F)\langle {}^1S_0 \| D^{(1)} \| {}^1P_1\rangle + c_{^3P_1}(F) \times \langle {}^1S_0 \| D^{(1)} \| {}^3P_1\rangle|^2, \quad (21)$$

where y refers to the $J=0$ or the $J=2$ state and the two c's are the mixing coefficients with $^1P_1$ and $^3P_1$, respectively. The mixing coefficients were calculated using first-order perturbation theory and were consequently given by

$$c_{^xP_1}(F) = \frac{\langle I^xP_1FM_F|\mathcal{H}_{hpf}|I^3P_yFM_F\rangle}{E(^3P_y)-E(^xP_1)}, \quad (22)$$

where x refers to the singlet or the triplet.

Using this and Eq. (11), the hyperfine-induced transition rate from $2s2p\,{}^3P_0$ to the ground state $2s^2\,{}^1S_0$ is given by

$$A_{hpf}(^1S_0,{}^3P_0) = \frac{(2\pi)^3}{9\hbar\lambda^3}I(I+1) \times \left|\frac{A(^1P_1,{}^3P_0)}{E(^3P_0)-E(^1P_1)}\langle {}^1S_0 \| D^{(1)} \| {}^1P_1\rangle + \frac{A(^3P_1,{}^3P_0)}{E(^3P_0)-E(^3P_1)}\langle {}^1S_0 \| D^{(1)} \| {}^3P_1\rangle\right|^2. \quad (23)$$

In the same way Eqs. (12) and (15) could be used to express the hyperfine-induced transition rate from $2s2p\,{}^3P_2$ to $2s^2\,{}^1S_0$ as

$$A_{hpf-E1}(^1S_0,{}^3P_2)=\frac{(2\pi)^3}{9\hbar\lambda^3}[(I+F+1)^2-4][4-(I-F)^2]\left|\frac{1}{E(^3P_2)-E(^1P_1)}\right.$$
$$\times\left[B(^1P_1,{}^3P_2)\sqrt{3}\frac{[F(F+1)-I(I+1)-3]}{4I(2I-1)}+\frac{A(^1P_1,{}^3P_2)}{2}\right]\langle{}^1S_0\|D^{(1)}\|{}^1P_1\rangle+\frac{1}{E(^3P_2)-E(^3P_1)}$$
$$\left.\times\left[B(^3P_1,{}^3P_2)\sqrt{3}\frac{[F(F+1)-I(I+1)-3]}{4I(2I-1)}+\frac{A(^3P_1,{}^3P_2)}{2}\right]\langle{}^1S_0\|D^{(1)}\|{}^3P_1\rangle\right|^2 \tag{24}$$

III. THE MCDHF METHOD

The calculations in this work were based on the multiconfiguration Dirac-Hartree-Fock method (MCDHF) [17], using the grasp2K relativistic atomic structure package [18]. The MCDHF method is based on the fundamental assumption that the atomic state function (ASF) $|\Gamma JM_J\rangle$, representing an atomic state, can be described as a linear combination of configuration state, functions (CSFs)

$$|\Gamma JM_J\rangle=\sum_i c_i|\gamma_i JM_J\rangle. \tag{25}$$

In turn, the CSFs are described by a sum of products of one-electron Dirac orbitals of the form

$$\phi(r,\theta,\varphi,\sigma)=\frac{1}{r}\begin{pmatrix}P(r)\chi_{\kappa m}(\theta,\varphi,\sigma)\\ iQ(r)\chi_{-\kappa m}(\theta,\varphi,\sigma)\end{pmatrix}, \tag{26}$$

where the angular and spin-dependent part are assumed to be known, but the radial part, $P(r)$ and $Q(r)$, remain to be determined.

Starting from the Dirac-Coulomb Hamiltonian

$$H_{DC}=\sum_i[c\alpha_i p_i+(\beta_i-1)c^2+V_i^N]+\sum_{i>j}\frac{1}{r_{ij}}, \tag{27}$$

where V_i^N is the monopole part of the electron-nucleus Coulomb interaction (CI), the ASFs were optimized in a self-consistent field procedure where both the radial part of the Dirac orbitals and the expansion coefficients c_i were optimized to self-consistency. In a subsequent CI calculation (McKenzie *et al.* [19]), the Breit interaction and QED effects were included.

From the ASFs a number of properties such as transition probabilities and hyperfine interaction constants were evaluated. The transition matrix elements can be expressed as reduced matrix elements of the form

$$\langle\Gamma J\|\mathbf{O}\|\Gamma' J'\rangle, \tag{28}$$

where **O** is the transition operator in the Babushkin or Coulomb gauge [20]. Some of the transitions were calculated between ASFs which were described by independently optimized sets of Dirac orbitals. To evaluate these transitions, biorthogonal transformation of the ASFs were performed [21] and in the new representation the matrix elements could be evaluated using standard Racah algebra.

IV. METHOD OF CALCULATION

Our calculations were based on the restricted active space (RAS) method (Roos *et al.* [22], Olsen *et al.* [23], Brage and Fischer [24]). The RAS method is an orbital driven technique where the calculations are enlarged in a systematic manner which is suitable for convergence studies of the calculations.

Separate optimizations were performed for the even and odd states. Beginning with the even, the ground state, we started by making a Dirac-Hartree-Fock calculation. We then extended our calculation stepwise by adding all single, double, triple, and quadruple (SDTQ) excitations from the reference configuration $1s^22s^2$ to a given set of orbitals which could be described as

$$\text{n2}=\{1s,2s,2p\},$$

$$\text{n3}=\text{n2}+\{3s,3p,3d\},$$

$$\text{n4}=\text{n3}+\{4s,4p,4d,4f\}.$$

Using the new configuration space, all new orbitals were optimized while the old were kept fixed. We then increased our calculations further by using the configuration list from step $n=4$ and added all single and double (SD) excitations from the multireference set $1s^22s^2$ and $1s^22p^2$ in the following steps:

$$\text{n5}=\text{n4}+\{5s,5p,5d,5f,5g\},$$

$$\text{n6}=\text{n5}+\{6s,6p,6d,6f,6g,6h\},$$

$$\text{n7}=\text{n6}+\{7s,7p,7d,7f,7g,7h,7i\}.$$

When optimizing the odd states, the levels belonging to the $2s2p$ configuration, we followed in principle the same steps as above. The main difference was that the first step after the Dirac-Hartree-Fock calculation was $n=3$ and we did not use any multireference set from $n=5$ and higher.

After optimizing the wave functions in each step, it was possible to evaluate hyperfine interaction constants and transition integrals. From these we could use the theory derived above to compute rates for hyperfine quenched and other transitions. Through the different steps of the calculations we monitored the convergence of different properties. After the final step, 7n, the Breit interaction and QED effects were added in a CI without reoptimization of the orbitals.

TABLE I. The calculated excitation energy of $2s2p\ ^3P_0$ and energies relative to the $^3P_0$ level in C^{2+}. All energies are given in cm^{-1}.

Step	$E_{^3P_0}$	$\Delta E_{^3P_1}$	$\Delta E_{^3P_2}$	$\Delta E_{^1P_1}$
n3	52697.85	34.27	102.95	52809.96
n4	52735.53	35.22	105.81	51631.29
n5	52600.06	34.79	104.51	50854.77
n6	52405.88	34.84	104.67	50581.75
n7	52387.46	34.84	104.68	50282.07
+Breit	52404.91	23.46	79.66	50262.18
Expt.[a]	52367.06	23.69	80.05	49984.98

[a]Ralchenko *et al.* [25].

V. RESULTS AND DISCUSSION

We use C^{2+} as an example of our computational methods. Table I shows a convergence study on the relevant energies and a comparison with experimental results taken from NIST Atomic Spectra Database (version 3.1.5) [25]. The fine structure of the $2s2p\ ^3P$ term as well as the excitation energy of the $2s2p\ ^3P_0$ level are almost totally converged. The term splitting between ^1P and ^3P shows a much slower convergence, but our result for the 7n calculation agrees with experiment to within 1%.

Table II shows a convergence study on the relevant transition rates. For the two electric dipole transition rates we present the results using both the Coulomb and the Babushkin gauge. The Babushkin gauge should be the most reliable of the two, but in principle they should give the same result for the exact wavefunction. The transition rates for the two gauges agree for the allowed $2s^2\ ^1S_0-2s2p\ ^1P_1$ transition, whereas there is a large discrepancy for the $2s^2\ ^1S_0-2s2p\ ^3P_1$ spin-forbidden transition. This has been observed for this type of transitions in earlier calculations and the conclusion is that the results from the Coulomb gauge are unreliable (Ynnerman and Froese Fischer [34] and Ellis [35]).

In Table III we compare our calculated lifetimes of the $2s2p^1P_1$ and the $^3P_1$ level to experiment. Lifetime measurements of the $^1P_1$ level has been performed for a range of ions studied in this work. Comparing our theoretical values to the experimental ones, agreement within the error bars is found.

TABLE III. Our calculated lifetimes of the $2s2p\ ^1P_1$ and the $^3P_1$ level compared to experimental values where available.

	$\tau(^1P_1)$ (ns)		$\tau(^3P_1)$ (ms)	
Ion	This work	Expt.	This work	Expt.
C^{2+}	0.562	0.57(2)[a]	9.84	9.714(13)[b]
N^{3+}	0.429	0.425(15)[c]	1.78	1.6(2)[d]
				1.73(1)[e]
O^{4+}	0.347	0.338(15)[c]	0.447	0.5(1)[d]
				0.432(9)[e]
Na^{7+}	0.218	0.21(1)[f]		
Mg^{8+}	0.193	0.190(15)[g]		
Al^{9+}	0.173	0.175(15)[g]		
Si^{10+}	0.155	0.150(12)[g]		
P^{11+}	0.140	0.140(10)[g]		
S^{12+}	0.128	0.129(6)[h]		
Cl^{13+}	0.116	0.117(10)[h]		

[a]Reistad *et al.* [26].
[b]Doerfert *et al.* [31].
[c]Engström *et al.* [27].
[d]Doerfert *et al.* [32].
[e]Träbert *et al.* [33].
[f]Tordoir *et al.* [28].
[g]Träbert and Heckmann [29].
[h]Bhattacharya *et al.* [30].

Much fewer experimental lifetimes are available for the $^3P_1$ level and comparison with experiment can only be done for C^{2+}, N^{3+}, and O^{4+}. Our theoretical lifetimes are slightly higher than the most accurate measurements, but we would argue that we are in agreement.

A. $2s2p\ ^3P_0$ hyperfine quenching

In Table IV we present the results for the hyperfine induced $2s^2\ ^1S_0-2s2p\ ^3P_0$ transition rate along the isoelectronic sequence, ranging from C^{2+} to Ti^{22+}, for all stable isotopes with a nonzero nuclear spin. We present two different results from our calculations, *ab initio* and *rescaled*, and compare with the theoretical results by Cheng *et al.* [3] and, where available, by Brage *et al.* [2]. In the *ab initio* approach

TABLE II. The convergence of transition rates of interest in C^{2+}. All rates are given in s^{-1} and $[x]$ represent 10^x.

	$A(^1S_0-^1P_1)$		$A(^1S_0-^3P_1)$		$A(\_S_0-^3P_2)$	$A(^3P_1-^3P_2)$
Step	C	B	C	B	$M2$	$M1$
n3	1.82053[9]	1.93108[9]	0.70696[2]	1.16436[2]	5.43787[−3]	4.36860[−6]
n4	1.70932[9]	1.83414[9]	0.87523[2]	1.32813[2]	5.40986[−3]	4.74313[−6]
n5	1.75914[9]	1.80485[9]	1.12594[2]	1.34021[2]	5.31035[−3]	4.57001[−6]
n6	1.74399[9]	1.77270[9]	1.13350[2]	1.34308[2]	5.19839[−3]	4.59169[−6]
n7	1.76954[9]	1.78000[9]	1.15901[2]	1.37948[2]	5.17123[−3]	4.59278[−6]
+Breit	1.76934[9]	1.78007[9]	1.79109[2]	1.01636[2]	5.16811[−3]	2.39417[−6]

TABLE IV. The hyperfine-induced electric dipole transition rates from $2s2p\ ^3P_0$ to $2s^2\ ^1S_0$ along the Be-like isoelectronic sequence. The rescaled results were obtained by rescaling the *ab initio* results to experimental energies [25]. The transition rates from this work are followed by two estimated errors obtained using the quadratic and the linear approach, see Sec. VI. All transition rates are given in s^{-1} and $[x]$ represent 10^x. RMBPT is relativistic many body perturbation theory.

				MCDF this work			
Z	Isotope	I	μ_I	*ab initio*	Rescaled	RMBPT[a]	MCHF[b]
6	^{13}C	1/2	0.7024	8.305[−4]4.4–7.5 %	8.266[−4]4.1–5.6 %	8.223[−4]	9.04[−4]
7	^{14}N	1	0.4038	4.453[−4]1.7–3.5 %	4.435[−4]1.3–2.0 %	4.440[−4]	4.92[−4]
7	^{15}N	1/2	−0.2832	3.285[−4]1.7–3.5 %	3.273[−4]1.3–2.0 %	3.269[−4]	3.62[−4]
8	^{17}O	5/2	−1.8938	1.478[−2]2.9–4.2 %	1.473[−2]2.8–3.6 %	1.488[−2]	1.52[−2]
9	^{19}F	1/2	2.6289	1.187[−1]1.4–2.4 %	1.182[−1]1.3–1.8 %	1.208[−1]	
10	^{21}Ne	3/2	−0.6618	7.527[−3]1.4–2.7 %	7.496[−3]0.74–1.1 %	7.453[−3]	6.54[−3][c]
11	^{23}Na	3/2	2.2175	1.433[−1]0.8−1.6 %	1.426[−1]0.60–0.91 %	1.431[−1]	1.28[−1][c]
12	^{25}Mg	5/2	−0.8554	2.893[−2]1.0–2.1 %	2.878[−2]0.54–0.82 %	2.871[−2]	2.72[−2][c]
13	^{27}Al	5/2	3.6415	8.136[−1]0.9–1.8 %	8.087[−1]0.52–0.79 %	8.094[−1]	8.13[−1][c]
14	^{29}Si	1/2	−0.5553	6.085[−2]1.1–2.3 %	6.043[−2]0.52–0.77 %	6.011[−2]	6.08[−2]
15	^{31}P	1/2	1.1316	3.687[−1]1.2–2.2 %	3.658[−1]0.51–0.76 %	3.648[−1]	
16	^{33}S	3/2	0.6438	9.439[−2]1.2–2.3 %	9.355[−2]0.52–0.75 %	9.315[−2]	
17	^{35}Cl	3/2	0.8219	2.145[−1]1.4–2.4 %	2.123[−2]0.53–0.75 %	2.113[−1]	
17	^{37}Cl	3/2	0.6841	1.486[−1]1.4–2.4 %	1.471[−1]0.53–0.75 %	1.464[−1]	
19	^{39}K	3/2	0.3915	8.974[−2]1.7–2.7 %	8.856[−2]0.60–0.80 %	8.873[−2]	1.24[−1][c]
19	^{40}K	4	−1.2981	7.399[−1]1.7–2.7 %	7.302[−1]0.60–0.80 %	7.314[−1]	1.02[0][c]
19	^{41}K	3/2	0.2149	2.704[−2]1.7–2.7 %	2.668[−2]0.60–0.80 %	2.673[−2]	3.97[−2][c]
20	^{43}Ca	7/2	−1.3173	1.040[0]1.9−2.7 %	1.025[0]0.65–0.85 %	1.021[0]	1.08[0][c]
21	^{45}Sc	7/2	5.7565	1.783[1]2.1–3.2 %	1.749[1]0.74–0.93 %	1.737[1]	
22	^{47}Ti	5/2	−0.7885	6.896[−1]2.3–3.3 %	6.774[−1]0.88–1.1 %	6.727[−1]	
22	^{49}Ti	7/2	−1.1042	1.242[0]2.3–3.3 %	1.220[0]0.88–1.1 %	1.212[0]	

[a]Cheng *et al.* [3].
[b]Brage *et al.* [2].
[c]Interpolated results.

we use pure ab initio calculations, while in the rescaled approach we use experimental values for two types of energy differences: first the transition energy and second the distance in energy from $^3P_0$ to the $^3P_1$ and $^1P_1$, respectively. The experimental energies are taken from the NIST Atomic Spectra Database (version 3.1.5) [25]. We have also estimated the uncertainty of each of the calculated hyperfine-induced transition rates using two different approaches, the quadratic and the linear approach (see Sec. VI for details). These uncertainties are presented after each transition rate, where the first value is from the quadratic approach and the second from the linear approach.

By just comparing the transition rates from the *ab initio* and the rescaled results, it is found that the latter are always lower. Adjusting the energies lowers the transition rate by less than 0.5% in the beginning of the isoelectronic sequence. This correction gradually increases in importance and for the higher members of the sequence investigated here, it decreases the rate by almost 2%. This trend may be explained by noting that for low-Z members of the sequence, the main change in transition rates when rescaling is due to inaccuracies in the energy splittings within the $2s2p$ configuration. This inaccuracy remains constant throughout the sequence. At the same time, the inaccuracy of the transition energy increases with Z. Adjusting the transition energy may be seen as less "intrusive," since we could argue that we still use *ab initio* line strengths.

Cheng *et al.* [3] used experimental energies from the NIST Atomic Spectra Database (version 3.1.5) [25] to calculate their hyperfine-induced transition rates. Their results should therefore be compared to our rescaled values. Such a comparison shows agreement to within 1% for all isotopes except ^{19}F where the difference is greater than 2%. Furthermore it is found that, with the exception of ^{19}F, our results are all in agreement with Cheng *et al.* [3] within our estimated uncertainties using both the quadratic and linear approaches. The disagreement for the ^{19}F results has no apparent explanation.

Our *ab initio* results also agree with the results of Cheng *et al.* [3] within the estimated uncertainties using the linear approach. The situation is not quite as good for the uncertainty estimates using the quadratic approach. Here our results do not agree with the results of Cheng *et al.* [3] within the estimated uncertainties for Sc^{17+} and Ti^{18+}. A more de-

tailed discussion of the uncertainty estimates is given in Sec. VI.

Brage *et al.* [2] performed calculations using the MCHF, the MCDHF, and the FCI methods to investigate a few isotopes along the Be-like isoelectronic sequence. They also used a fitting procedure to interpolate the hyperfine-induced transition rates of some other ions and we have marked the latter with an asterix in Table IV. Comparing the noninterpolated results by Brage *et al.* with ours and Cheng *et al.* [3], agreement is found except for the two first ions. For these Brage *et al.* predict a transition rate which is about 10% higher than those predicted in our work and in the work of Cheng *et al.* [3]. Making the same comparisons with the interpolated results, a scattered pattern is found and the predicted transition rates by Brage *et al.* range from being about 15% lower to 40% higher than those predicted in our work and in the work of Cheng *et al.* [3].

In a recent experiment by Schippers *et al.* [4], the hyperfine-induced transition rate of the $2s^2\ ^1S_0-2s2p\ ^3P_0$ transition for $^{47}Ti^{18+}$ was determined to be 0.56(3) s^{-1}. This rate is about 17% smaller than the predicted value in both this work and Cheng *et al.* [3]. From observations of the planetary nebula NGC3918, Brage *et al.* [5] experimentally determined the hyperfine-induced transition rate for an admixture of $^{14}N^{3+}$ and $^{15}N^{3+}$ to be $4\times10^{-4}\pm33\%$ s^{-1}, in agreement with the results from this work and from Cheng *et al.* [3]. Unfortunately, the accuracy of this measurement is not good enough to rule out a similar disagreement as found by Schippers *et al.* [4].

B. $2s2p\ ^3P_2$ hyperfine quenching

In Table V we present the results from the *ab initio* calculations for the $2s2p\ ^3P_2$ hyperfine levels along the isoelectronic sequence. Besides giving the hyperfine-induced transition rates we also give the $M2$ rate to the ground state and the $M1$ rate to the $2s2p\ ^3P_1$ level. The rates of the two $E2$ transitions within the multiplet are several orders of magnitude smaller than the two magnetic multipole rates for all members of the sequence investigated in this work and are omitted. We also give the hyperfine-dependent lifetimes of $^3P_2$ and the branching fractions, Q_A of the $2s^2\ ^1S_0-2s2p\ ^3P_2$ transition. Each atomic property is followed by the estimated uncertainty from the linear approach.

By investigating the results in Table V it is found that the $^3P_0$ hyperfine level has a stronger quenching than the $^3P_2$ hyperfine levels in the beginning of the sequence. The quenching of the $^3P_2$ hyperfine levels however increases faster with Z, and beyond ^{29}Si at least one hyperfine level of $^3P_2$ has a stronger quenching than $^3P_0$.

We will discuss the results in six different sections: (1) the influence of the hyperfine quenching on the lifetime, (2) the importance of the nuclear electric quadrupole hyperfine interaction, (3) the hyperfine induced transition rate relative to the $M2$ rate, (4) the hyperfine-induced transition rate relative to the $M1$ rate, (5) hyperfine-dependent branching fractions, and (6) the relative importance of the hyperfine mixing with $2s2p\ ^3P_1$ and $^1P_1$.

1. Hyperfine-level-dependent lifetimes

In an isotope without a nuclear spin, the lifetime of the $2s2p\ ^3P_2$ level is determined by the $M1$ and $M2$ transition rates. In Fig. 1 we plot the hyperfine-dependent lifetimes relative to the lifetime in the absence of a nuclear spin along the isoelectronic sequence. Depending on nuclear spin I, there is always one or two hyperfine levels which are not hyperfine quenched and the lifetime of these are therefore equal to the lifetime of the level in an isotope without nuclear spin. It is found that in spite of the fact that most isotopes do not show a large hyperfine dependence of the lifetimes of the $^3P_2$ hyperfine levels, there are important exceptions. As a matter of fact, the lifetimes of the two hyperfine levels of $^{19}F^{5+}$ differ by more than 300%. By investigating the behavior along the sequence, it is apparent that the importance of the hyperfine quenching is decreasing with increasing Z. As an example, the F-dependent lifetimes in ^{45}Sc differ by as little as 5% even though the nuclear magnetic dipole moment of this isotope is very large, $\mu_I=4.7565$ nuclear magnetons.

2. The nuclear electric quadrupole hyperfine interaction

In some earlier work, the nuclear electric quadrupole hyperfine interaction was left out in the calculations of hyperfine quenching. We will therefore investigate the importance of this effect, relative the nuclear magnetic dipole hyperfine interaction. By eliminating the electric quadrupole interaction from Eq. (24), we could calculate the nuclear magnetic dipole hyperfine-induced transition rate A_{hpf}^{M1} from

$$A_{hpf}^{M1}(^1S_0,{}^3P_2)=\frac{(2\pi)^3}{18\hbar\lambda^3}[(I+F+1)^2-4][4-(I-F)^2]\times\left|\frac{A(^1P_1,{}^3P_2)}{E(^3P_2)-E(^1P_1)}\langle{}^1S_0\|D^{(1)}\|{}^1P_1\rangle+\frac{A(^3P_1,{}^3P_2)}{E(^3P_2)-E(^3P_1)}\langle{}^1S_0\|D^{(1)}\|{}^3P_1\rangle\right|^2. \tag{29}$$

In Fig. 2 we have plotted the total hyperfine-induced transition rate A_{hpf} relative to A_{hpf}^{M1}. This relative rate tells us how much the electric quadrupole interaction increase or decrease the total hyperfin-induced rate. It is found that the electric quadrupole interaction in most cases changes the rate with a few percent, but there are examples of changes as big as 8%. Even if the effect is rather small, it is still important that it is included if accurate theoretical predictions are to be made.

3. A_{hpf} relative to A_{M2}

In Fig. 3 we have plotted the hyperfine-induced transition rate, A_{hpf}, relative to the magnetic quadrupole transition rate, A_{M2}, along the isoelectronic sequence, indicating which channel dominates the decay to the ground state. There is no obvious Z dependence for this relative rate and the dominant transition channel seems to depend only on the size of the electromagnetic multipole moments of the nucleus. All along the sequence there are hyperfine levels which decay mainly to the ground state through the hyperfine-induced electric dipole transition channel. However, there are always one or two hyperfine levels which have no hyperfine-induced transition channel.

TABLE V. The results for the $2s2p\ ^3P_2$ hyperfine levels along the Be-like isoelectronic sequence. Each transition rate A, lifetime τ, and branching fraction Q_A is followed by the estimated uncertainty using the linear approach (see Sec. VI). $[x]$ represent 10^x.

F_i	A_{hpf} (s^{-1})	A_{M2} (s^{-1})	A_{M1} (s^{-1})	τ (s)	Q_A
^{13}C, $I=1/2$, $\mu_I=0.7024$, Q=0					
3/2	7.374[−4] 3.9%	5.168[−3] 0.82%	2.394[−6] 0.85%	1.693[2] 1.2%	9.996[−1] 0.00084%
5/2	0.0	5.168[−3] 0.82%	2.394[−6] 0.85%	1.934[2] 0.82%	9.995[−1] 0.00078%
^{14}N, $I=1$, $\mu_I=0.4038$, $Q=0.0156$					
1	2.185[−4] 2.2%	1.149[−2] 0.27%	3.999[−5] 0.67%	8.515[1] 0.31%	9.966[−1] 0.0033%
2	3.887[−4] 2.2%	1.149[−2] 0.27%	3.999[−5] 0.67%	8.393[1] 0.34%	9.966[−1] 0.0034%
3	0.0	1.149[−2] 0.27%	3.999[−5] 0.67%	8.676[1] 0.27%	9.965[−1] 0.0033%
^{15}N, $I=1/2$, $\mu_I=-0.2832$, $Q=0$					
3/2	3.196[−4] 2.2%	1.149[−2] 0.27%	3.999[−5] 0.67%	8.442[1] 0.32%	9.966[−1] 0.0033%
5/2	0.0	1.149[−2] 0.27%	3.999[−5] 0.67%	8.676[1] 0.27%	9.965[−1] 0.0033%
^{17}O, $I=5/2$, $\mu_I=-1.8938$, $Q=-0.02578$					
1/2	0.0	2.160[−2] 0.29%	3.841[−4] 1.3%	4.549[1] 0.31%	9.825[−1] 0.027%
3/2	5.498[−3] 2.5%	2.160[−2] 0.29%	3.841[−4] 1.3%	3.639[1] 0.75%	9.860[−1] 0.028%
5/2	1.116[−2] 2.5%	2.160[−2] 0.29%	3.841[−4] 1.3%	3.018[1] 1.1%	9.884[−1] 0.027%
7/2	1.174[−2] 2.5%	2.160[−2] 0.29%	3.841[−4] 1.3%	2.965[1] 1.1%	9.886[−1] 0.027%
9/2	0.0	2.160[−2] 0.29%	3.841[−4] 1.3%	4.549[1] 0.31%	9.825[−1] 0.027%
^{19}F, $I=1/2$, $\mu_I=2.6289$, $Q=0$					
3/2	1.282[−1] 1.8%	3.657[−2] 0.48%	2.558[−3] 1.2%	5.975[0] 1.5%	9.847[−1] 0.042%
5/2	0.0	3.657[−2] 0.48%	2.558[−3] 1.2%	2.555[1] 0.53%	9.346[−1] 0.11%
^{21}Ne, $I=3/2$, $\mu_I=-0.6618$, $Q=0.1029$					
1/2	1.624[−3] 1.4%	5.772[−2] 0.47%	1.312[−2] 1.0%	1.380[1] 0.60%	8.190[−1] 0.28%
3/2	5.307[−3] 1.4%	5.772[−2] 0.47%	1.312[−2] 1.0%	1.313[1] 0.64%	8.277[−1] 0.27%
5/2	7.211[−3] 1.4%	5.772[−2] 0.47%	1.312[−2] 1.0%	1.281[1] 0.65%	8.319[−1] 0.27%
7/2	0.0	5.772[−2] 0.47%	1.312[−2] 1.0%	1.412[1] 0.58%	8.148[−1] 0.28%
^{23}Na, $I=3/2$, $\mu_I=2.2175$, $Q=0.101$					
1/2	3.391[−2] 1.3%	8.669[−2] 0.59%	5.526[−2] 1.0%	5.686[0] 0.87%	6.858[−1] 0.57%
3/2	1.078[−1] 1.3%	8.669[−2] 0.59%	5.526[−2] 1.0%	4.003[0] 1.0%	7.788[−1] 0.45%
5/2	1.401[−1] 1.3%	8.669[−2] 0.59%	5.526[−2] 1.0%	3.546[0] 1.0%	8.040[−1] 0.41%
7/2	0.0	8.669[−2] 0.59%	5.526[−2] 1.0%	7.044[0] 0.76%	6.107[−1] 0.63%
^{25}Mg, $I=5/2$, $\mu_I=-0.8554$, $Q=0.22$					
1/2	0.0	1.256[−1] 0.77%	1.998[−1] 0.39%	3.073[0] 0.54%	3.860[−1] 0.71%
3/2	1.203[−2] 1.2%	1.256[−1] 0.77%	1.998[−1] 0.39%	2.963[0] 0.57%	4.079[−1] 0.71%
5/2	2.521[−2] 1.2%	1.256[−1] 0.77%	1.998[−1] 0.39%	2.852[0] 0.59%	4.301[−1] 0.71%
7/2	2.774[−2] 1.2%	1.256[−1] 0.77%	1.998[−1] 0.39%	2.832[0] 0.59%	4.342[−1] 0.70%
9/2	0.0	1.256[−1] 0.77%	1.998[−1] 0.39%	3.073[0] 0.54%	3.860[−1] 0.71%
^{27}Al, $I=5/2$, $\mu_I=3.6415$, $Q=0.14$					
1/2	0.0	1.772[−1] 0.95%	6.393[−1] 0.87%	1.225[0] 0.89%	2.170[−1] 1.4%
3/2	3.724[−1] 1.3%	1.772[−1] 0.95%	6.393[−1] 0.87%	8.411[−1] 1.0%	4.623[−1] 1.1%
5/2	7.532[−1] 1.3%	1.772[−1] 0.95%	6.393[−1] 0.87%	6.370[−1] 1.1%	5.927[−1] 0.87%
7/2	7.893[−1] 1.3%	1.772[−1] 0.95%	6.393[−1] 0.87%	6.227[−1] 1.1%	6.019[−1] 0.85%
9/2	0.0	1.772[−1] 0.95%	6.393[−1] 0.87%	1.225[0] 0.89%	2.170[−1] 1.4%
^{29}Si, $I=1/2$, $\mu_I=-0.5553$, $Q=0$					
3/2	8.009[−2] 1.4%	2.452[−1] 1.1%	1.851[0] 0.78%	4.595[−1] 0.84%	1.495[−1] 1.7%
5/2	0.0	2.452[−1] 1.1%	1.851[0] 0.78%	4.771[−1] 0.82%	1.170[−1] 1.7%
^{31}P, $I=1/2$, $\mu_I=1.1316$, $Q=0$					
3/2	5.077[−1] 1.4%	3.343[−1] 1.3%	4.930[0] 0.47%	1.733[−1] 0.60%	1.459[−1] 1.6%
5/2	0.0	3.343[−1] 1.3%	4.930[0] 0.47%	1.900[−1] 0.52%	6.351[−2] 1.6%
^{33}S, $I=3/2$, $\mu_I=0.6438$, $Q=-0.064$					

TABLE V. (*Continued.*)

F_i	A_{hpf} (s^{-1})	A_{M2} (s^{-1})	A_{M1} (s^{-1})	τ (s)	Q_A
1/2	2.650[−2] 1.5%	4.512[−1] 1.5%	1.224[1] 0.55%	7.864[−2] 0.59%	3.756[−2] 2.0%
3/2	8.610[−2] 1.5%	4.512[−1] 1.5%	1.224[1] 0.55%	7.827[−2] 0.59%	4.205[−2] 2.0%
5/2	1.158[−1] 1.5%	4.512[−1] 1.5%	1.224[1] 0.55%	7.809[−2] 0.60%	4.428[−2] 2.0%
7/2	0.0	4.512[−1] 1.5%	1.224[1] 0.55%	7.880[−2] 0.59%	3.555[−2] 2.1%
^{35}Cl, I=3/2, μ_I=0.8219, Q=−0.08249					
1/2	6.351[−2] 1.6%	6.044[−1] 1.7%	2.861[1] 0.60%	3.415[−2] 0.63%	2.281[−2] 2.3%
3/2	2.064[−1] 1.6%	6.044[−1] 1.7%	2.861[1] 0.60%	3.399[−2] 0.64%	2.756[−2] 2.2%
5/2	2.779[−1] 1.6%	6.044[−1] 1.7%	2.861[1] 0.60%	3.391[−2] 0.64%	2.991[−2] 2.2%
7/2	0.0	6.044[−1] 1.7%	2.861[1] 0.60%	3.423[−2] 0.63%	2.069[−2] 2.3%
F_i	A_{hpf-E1} (s^{-1})	A_{M2} (s^{-1})	A_{M1} (s^{-1})	τ (s)	Q_A
^{37}Cl, I=3/2, μ_I=0.6841, Q=−0.06493					
1/2	4.407[−2] 1.6%	6.044[−1] 1.7%	2.861[1] 0.60%	3.418[−2] 0.63%	2.216[−2] 2.4%
3/2	1.431[−1] 1.6%	6.044[−1] 1.7%	2.861[1] 0.60%	3.406[−2] 0.63%	2.546[−2] 2.3%
5/2	1.924[−1] 1.6%	6.044[−1] 1.7%	2.861[1] 0.60%	3.400[−2] 0.63%	2.709[−2] 2.3%
7/2	0.0	6.044[−1] 1.7%	2.861[1] 0.60%	3.423[−2] 0.63%	2.069[−2] 2.3%
^{39}K, I=3/2, μ_I=0.3915, Q=0.049					
1/2	3.217[−2] 1.8%	1.071[0] 2.3%	1.346[2] 0.060%	7.368[−3] 0.077%	8.127[−3] 2.3%
3/2	1.010[−1] 1.8%	1.071[0] 2.3%	1.346[2] 0.060%	7.364[−3] 0.078%	8.630[−3] 2.3%
5/2	1.284[−1] 1.8%	1.071[0] 2.3%	1.346[2] 0.060%	7.363[−3] 0.079%	8.830[−3] 2.3%
7/2	0.0	1.071[0] 2.3%	1.346[2] 0.060%	7.369[−3] 0.077%	7.892[−3] 2.3%
^{41}K, I=8/2, μ_I=−1.2981, Q=−0.061					
2	0.0	1.071[0] 2.3%	1.346[2] 0.060%	7.369[−3] 0.077%	7.892[−3] 2.3%
3	5.788[−1] 1.8%	1.071[0] 2.3%	1.346[2] 0.060%	7.338[−3] 0.085%	1.211[−2] 2.1%
4	9.850[−1] 1.8%	1.071[0] 2.3%	1.346[2] 0.060%	7.316[−3] 0.090%	1.504[−2] 2.1%
5	9.147[−1] 1.8%	1.071[0] 2.3%	1.346[2] 0.060%	7.320[−3] 0.089%	1.453[−2] 2.1%
6	0.0	1.071[0] 2.3%	1.346[2] 0.060%	7.369[−3] 0.077%	7.892[−3] 2.3%
^{41}K, I=3/2, μ_I=0.2149, Q=0.06					
1/2	1.015[−2] 1.8%	1.071[0] 2.3%	1.346[2] 0.060%	7.369[−3] 0.077%	7.966[−3] 2.3%
3/2	3.115[−2] 1.8%	1.071[0] 2.3%	1.346[2] 0.060%	7.368[−3] 0.077%	8.120[−3] 2.3%
5/2	3.807[−2] 1.8%	1.071[0] 2.3%	1.346[2] 0.060%	7.367[−3] 0.078%	8.170[−3] 2.3%
7/2	0.0	1.071[0] 2.3%	1.346[2] 0.060%	7.369[−3] 0.077%	7.892[−3] 2.3%
^{43}Ca, I=7/2, μ_I=−1.3173, Q=−0.062					
3/2	0.0	1.422[0] 2.4%	2.742[2] 1.4%	3.628[−3] 1.4%	5.158[−3] 3.8%
5/2	8.310[−1] 2.0%	1.422[0] 2.4%	2.742[2] 1.4%	3.617[−3] 1.4%	8.148[−3] 3.6%
7/2	1.469[0] 2.0%	1.422[0] 2.4%	2.742[2] 1.4%	3.609[−3] 1.4%	1.043[−2] 3.6%
9/2	1.404[0] 2.0%	1.422[0] 2.4%	2.742[2] 1.4%	3.610[−3] 1.4%	1.020[−2] 3.6%
11/2	0.0	1.422[0] 2.4%	2.742[2] 1.4%	3.628[−3] 1.4%	5.158[−3] 3.8%

TABLE V. (*Continued.*)

F_i	A_{hpf} (s^{-1})	A_{M2} (s^{-1})	A_{M1} (s^{-1})	τ (s)	Q_A
^{45}Sc, $I=7/2$, $\mu_I=4.7565$, $Q=-0.22$					
3/2	0.0	1.887[0] 2.6%	5.390[2] 0.66%	1.849[−3] 0.67%	3.489[−3] 3.3%
5/2	1.506[1] 2.1%	1.887[0] 2.6%	5.390[2] 0.66%	1.799[−3] 0.71%	3.047[−2] 2.8%
7/2	2.691[1] 2.1%	1.887[0] 2.6%	5.390[2] 0.66%	1.761[−3] 0.74%	5.072[−2] 2.7%
9/2	2.609[1] 2.1%	1.887[0] 2.6%	5.390[2] 0.66%	1.764[−3] 0.74%	4.935[−2] 2.7%
11/2	0.0	1.887[0] 2.6%	5.390[2] 0.66%	1.849[−3] 0.67%	3.489[−3] 3.3%
^{47}Ti, $I=5/2$, $\mu_I=-0.7885$, $Q=0.29$					
1/2	0.0	2.508[0] 2.8%	1.026[3] 0.60%	9.721[−4] 0.61%	2.438[−3] 3.4%
3/2	4.952[−1] 2.3%	2.508[0] 2.8%	1.026[3] 0.60%	9.717[−4] 0.61%	2.918[−3] 3.3%
5/2	1.057[0] 2.3%	2.508[0] 2.8%	1.026[3] 0.60%	9.711[−4] 0.61%	3.462[−3] 3.3%
7/2	1.192[0] 2.3%	2.508[0] 2.8%	1.026[3] 0.60%	9.710[−4] 0.61%	3.592[−3] 3.2%
9/2	0.0	2.508[0] 2.8%	1.026[3] 0.60%	9.721[−4] 0.61%	2.438[−3] 3.4%
^{49}Ti, $I=7/2$, $\mu_I-1.1042$, $Q=0.24$					
3/2	0.0	2.508[0] 2.8%	1.026[3] 0.60%	9.721[−4] 0.61%	2.438[−3] 3.4%
5/2	1.105[0] 2.3%	2.508[0] 2.8%	1.026[3] 0.60%	9.711[−4] 0.61%	3.508[−3] 3.3%
7/2	2.018[0] 2.3%	2.508[0] 2.8%	1.026[3] 0.60%	9.702[−4] 0.61%	4.391[−3] 3.2%
9/2	2.009[0] 2.3%	2.508[0] 2.8%	1.026[3] 0.60%	9.702[−4] 0.61%	4.383[−3] 3.2%
11/2	0.0	2.508[0] 2.8%	1.026[3] 0.60%	9.721[−4] 0.61%	2.438[−3] 3.4%

To obtain a better picture of the trend along the sequence, it would be desirable to define a "reduced" hyperfine-induced transition rate independent of the nuclear part of the wave function. This could in principle be done in two steps. Eliminating all I and F dependence from the expression for the hyperfine-induced transition rate. Defining hyperfine interaction constants which are only dependent on the electronic part of the wave function and replacing the real hyperfine constants with these electronic ones. This is not possible to do for the total rate, since the magnetic dipole and electric quadrupole contributions in Eq. (24) have different I and F dependence. In the last section we saw that the contribution from the latter is small, and we therefore neglect the quadrupole contribution and use Eq. (29) when defining an "electronic" rate A_{hpf}^{elec}. By eliminating the I and F dependence from Eq. (29) and replacing the hyperfine interaction constants by their electronic counterpart defined as

$$A^{elec} = \frac{I}{\mu_I} A, \tag{30}$$

we can extract the nuclear and F dependence as

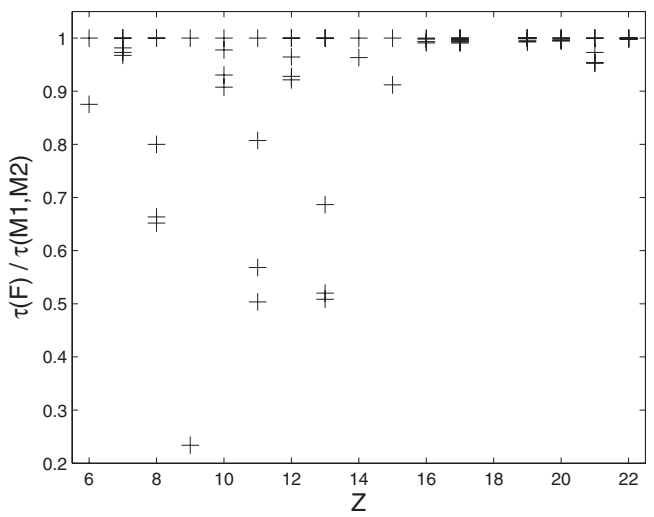

FIG. 1. Hyperfine level dependent lifetimes of $2s2p\ ^3P_2$ relative to the lifetime of the level in an isotope with zero nuclear spin.

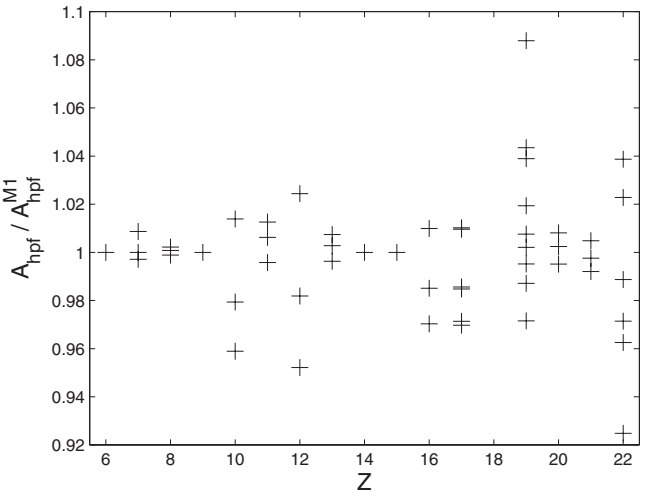

FIG. 2. Contribution from the nuclear electric quadrupole hyperfine interaction to the hyperfine-induced transition rate, plotted as A_{hpf} relative to A_{hpf}^{M1} (see text).

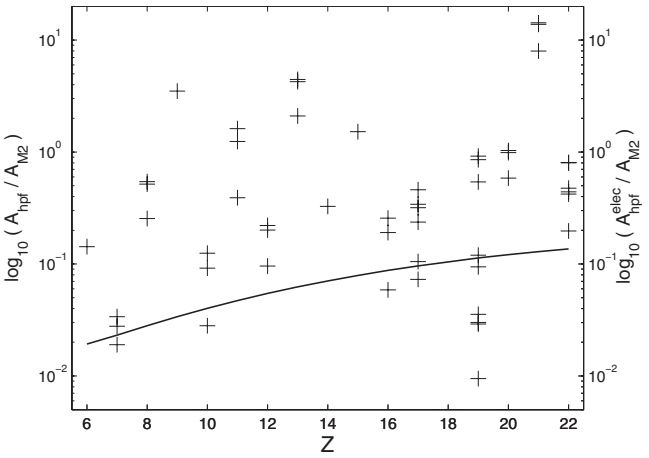

FIG. 3. A_{hpf} relative to A_{M2} along the isoelectronic sequence on a logarithmic scale. The solid line, A_{hpf}^{elec} relative to A_{M2} (see text).

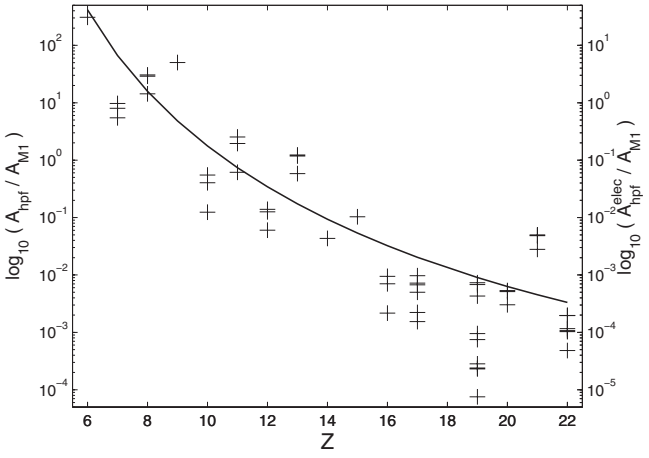

FIG. 4. A_{hpf} relative A_{M1} along the isoelectronic sequence on a logarithmic scale. The solid line, A_{hpf}^{elec} relative A_{M1} (see text).

$$A_{hpf}^{elec}({}^1S_0, {}^3P_2) = \frac{(2\pi)^3}{18\hbar\lambda^3} \times \left| \frac{A^{elec}({}^1P_1, {}^3P_2)}{E({}^3P_2) - E({}^1P_1)} \langle {}^1S_0 \| D^{(1)} \| {}^1P_1 \rangle + \frac{A^{elec}({}^3P_1, {}^3P_2)}{E({}^3P_2) - E({}^3P_1)} \langle {}^1S_0 \| D^{(1)} \| {}^3P_1 \rangle \right|^2 . \quad (31)$$

To investigate the Z dependence of the hyperfine-induced transition rate relative to the $M2$ rate, we have plotted A_{hpf}^{elec} relative to A_{M2} along the isoelectronic sequence in Fig. 3. It is found that A_{hpf}^{elec} has a slightly stronger Z dependence than A_{M2}, but the relative rate increases by less than one order of magnitude over the whole sequence. Andersson *et al.* [14] performed a similar study for the A_{hpf}^{elec} and A_{M2} rates of the $4s^2\ {}^1S_0 - 4s4p\ {}^3P_2$ transition in the Zn-like isoelectronic sequence. In the Zn sequence they found basically no Z dependence of relative size of the two rates, in agreement with what would be expected from a Z-dependence analysis (see Andersson *et al.* [14]).

4. A_{hpf} relative to A_{M1}

In Fig. 4 we have plotted the hyperfine-induced rate A_{hpf}, as well as the "reduced" hyperfine-induced rate A_{hpf}^{elec}, of the $2s^2\ {}^1S_0 - 2s2p\ {}^3P_2$ transition, relative to the $M1$ rate, A_{M1}, of the $2s2p\ {}^3S_1 - 2s2p\ {}^3P_2$ transition along the isoelectronic sequence. From this plot it is found that the $M1$ rate has a much stronger Z dependence than the hyperfine-induced transition. Even if the latter dominates in the beginning of the sequence, the roles are reversed towards the end. The same is true in a comparison between the $M2\ {}^1S_0 - {}^3P_2$ and $M1\ {}^3P_1 - {}^3P_2$ transitions, where the former dominates in the beginning and the latter at the end of the sequence. The $M1$ rate becomes larger than the $M2$ in Mg^{8+} and as a consequence the hyperfine interaction sensitivity of the lifetimes decreasing rather quickly from there on along the sequence.

5. Branching fraction

The relative intensity between the two lines $2s^2\ {}^1S_0 - 2s2p\ {}^3P_2$ and $2s2p\ {}^3P_1 - 2s2p\ {}^3P_2$ in a spectrum can be described by the branching fraction of the two transitions. In the presence of a nuclear spin, the branching fraction Q_A of the former line is given by

$$Q_A = \frac{A_{M2} + A_{hpf}}{A_{M1} + A_{M2} + A_{hpf}}.$$

We have plotted the hyperfine-level-dependent branching fraction along the isoelectronic sequence in Fig. 5. The solid line in the same figure is the branching fraction for an isotope with zero nuclear spin. As pointed out before there are always one or two hyperfine levels which are not hyperfine quenched and their branching fractions therefore coincide with this line. From the figure it is found that in the spectrum of a few isotopes there could be some major intensity redistribution from the $2s2p\ {}^3P_1 - 2s2p\ {}^3P_2$ to the $2s^2\ {}^1S_0 - 2s2p\ {}^3P_2$ line due to the hyperfine quenching. As an example, even if the hyperfine quenching has a very small impact on the lifetime of the hyperfine levels of ^{45}Sc, the quenching could manifest itself as a very weak line from the $2s^2\ {}^1S_0 - 2s2p\ {}^3P_2$ transition. Excluding hyperfine quenching

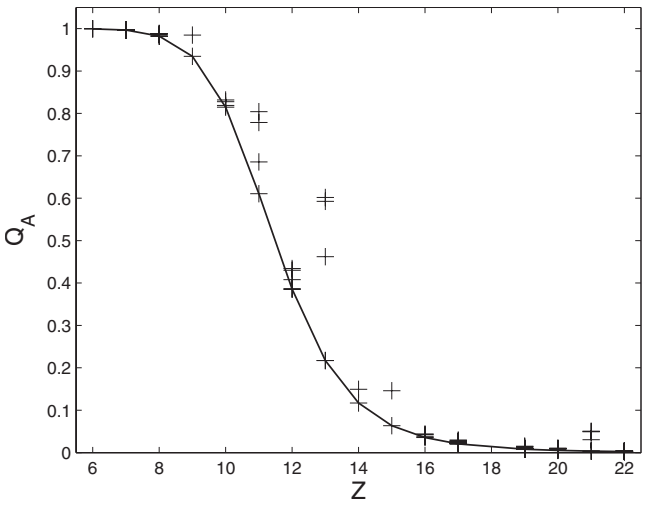

FIG. 5. The F-dependent branching fraction, Q_A, of the $2s^2\ {}^1S_0 - 2s2p\ {}^3P_2$ transition along the isoelectronic sequence. The solid line is Q_A in the absence of a nuclear spin.

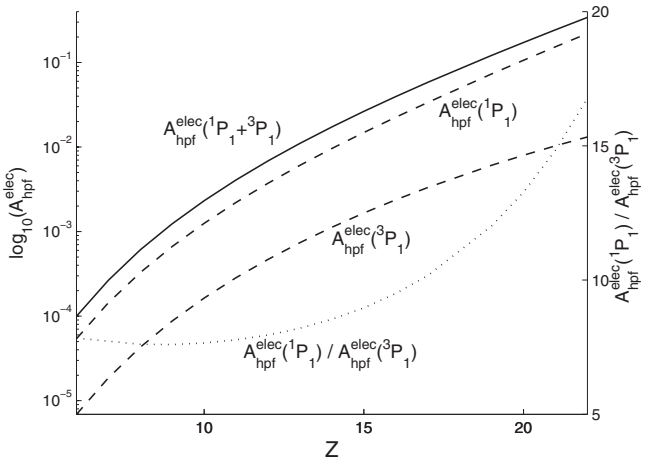

FIG. 6. The importance of including the mixing with $^1P_1$, respectively, $^3P_1$. The different electronic transition rates A_{hpf}^{elec} plotted on a logarithmic scale (left y axis) and $A_{hpf}^{elec}(^1P_1)$ relative to $A_{hpf}^{elec}(^3P_1)$ plotted on a linear scale (right y axis).

from the theoretical model would predict that this line should not be possible to see in the spectrum.

6. The importance of including mixing with $^3P_1$

Both Brage *et al.* [2] and Cheng *et al.* [3] showed that it is important to include both the mixing with $^3P_1$ and $^1P_1$ to calculate the hyperfine quenching of the $^3P_0$ level accurately. They also showed that the importance of including the mixing with $^1P_1$ decreases along the isoelectronic sequence. We have performed a similar study for the quenching of the $^3P_2$ level. Excluding the hyperfine mixing due to the electric quadrupole hyperfine interaction, the electronic hyperfine-induced transition rate A_{hpf}^{elec}, defined in Eq. (31), were calculated including mixing only with $^3P_1$, $A_{hpf}^{elec}(^3P_1)$, and $^1P_1$, $A_{hpf}^{elec}(^1P_1)$, respectively. Figure 6 shows the results along the isoelectronic sequence, also shown are the results including the mixing with both. To obtain a clearer picture of the trend along the sequence, we have also plotted the relative transition rate between $A_{hpf}^{elec}(^3P_1)$ and $A_{hpf}^{elec}(^1P_1)$ on a linear scale (the right vertical axis in the figure). From this figure it is clear that hyperfine mixing with both states are important all along the sequence studied here, but the importance of the mixing with the $^3P_1$ level decreases towards the end.

VI. UNCERTAINTY ESTIMATE

A. Method

There is no well-established theory for estimating the uncertainty of theoretically predicted atomic properties. Our approach is not built on strong theoretical arguments but should rather be seen as a first-order model. The approach is only valid under the assumption that the model used for calculating the atomic properties has no systematic errors.

In this paper we are interested in the hyperfine-induced transitions from $2s2p\ ^3P_0$ and $^3P_2$ to the ground state. We are also interested in comparing the latter of these two with the $M2$ transition to the ground state and the $M1$ transition to $2s2p\ ^3P_1$. It is therefore necessary to estimate not only the uncertainty of the hyperfine-induced electric dipole transition rates but also the uncertainties of the $M1$ and $M2$ rates.

Starting with the two magnetic multipole transitions, we can express these transition rates as

$$A = (E_{tr})^{2k+1} S, \tag{32}$$

where k is the rank of the multipole transition operator, E_{tr} is the transition energy, and S is the line strength. Having this type of dependence on E_{tr} and S, the uncertainty of the transition rate can be written as

$$\delta A = \sqrt{[(2k+1)\delta E]^2 + (\delta S)^2}. \tag{33}$$

To use this quadratic form for calculating the uncertainty, the different parameters should be independent of each other. This is not obvious here since both the energy and the line strength are based on the same wave functions. We therefore also calculated the uncertainties using a linear formula, i.e.,

$$\delta A = (2k+1)|\delta E| + |\delta S| \tag{34}$$

and label the former the quadratic error and the latter the linear error.

The uncertainty of the transition energy was easily obtained by comparing our theoretical value to experiment using the NIST Atomic Spectra Database (version 3.1.5) [25]. To estimate the uncertainty of the line strength we used an approach we call the *convergence method*. In this method we studied how the line strength converged when the calculations were expanded. For each line strength, we tried to find a $\mathcal{K}$ such that the relation

$$\mathcal{K}(S_{ni} - S_{n(i-1)}) \geqslant (S_{n7} - S_{ni}) \tag{35}$$

were fulfilled for all i and where ni are the different steps in our calculations. From this we found it reasonable to assume that the fully converged results should not differ by more than

$$\delta S = S_{n\infty} - S_{n7} \leqslant \mathcal{K}(S_{n7} - S_{n6}) \tag{36}$$

from our final result.

Estimating the uncertainty of the hyperfine-induced transitions is a bit more complicated. Starting with the hyperfine-induced transition from $2s2p\ ^3P_0$ we could rewrite Eq. (23) as

$$A_{hpf}(^1S_0, ^3P_0) = (E_{tr})^3 I(I+1) \left| \frac{A_{^1P_1}}{\Delta E_{^1P_1}} S_{^1P_1}^{1/2} + \frac{A_{^3P_1}}{\Delta E_{^3P_1}} S_{^3P_1}^{1/2} \right|^2, \tag{37}$$

where E_{tr} is the transition energy, ΔE is the energy differences of $^3P_1$ and $^1P_1$, respectively, relative to $^3P_0$, A's are the magnetic dipole hyperfine interaction constants, and S's are the line strengths for the transitions from $^1P_1$ and $^3P_1$ to the ground state. Working out the square of this expression, the transition rate can be expressed as a sum over three terms where one only depends on the mixing with $2s2p\ ^1P_1$, one only on the mixing with $^3P_1$, and one on the mixing with both. We denote these terms $\mathcal{A}_{^1P_1}$, $\mathcal{A}_{^3P_1}$, and $\mathcal{A}_{mix}$, and by

using the linear approach to calculate the uncertainty in these we obtain

$$\delta\mathcal{A}_{^1P_1} = 3|\delta E_{tr}| + 2|\delta A_{^1P_1}| + 2|\delta\Delta E_{^1P_1}| + |\delta S_{^1P_1}|,$$

$$\delta\mathcal{A}_{mix} = 3|\delta E_{tr}| + |\delta A_{^1P_1}| + |\delta A_{^3P_1}| + |\delta\Delta E_{^1P_1}| + |\delta\Delta E_{^3P_1}| + (|\delta S_{^1P_1}| + |\delta S_{^3P_1}|)/2,$$

$$\delta\mathcal{A}_{^3P_1} = 3|\delta E_{tr}| + 2|\delta A_{^3P_1}| + 2|\delta\Delta E_{^3P_1}| + |\delta S_{^3P_1}|. \quad (38)$$

In a similar way we obtain uncertainty expressions for the quadratic error. Using any of the two approaches, the uncertainty of $A_{hpf}(^1S_0, ^3P_0)$ is then given by

$$\delta A_{hpf}(^1S_0, ^3P_0) = \alpha_{^1P_1}\mathcal{A}_{^1P_1} + \alpha_{mix}\mathcal{A}_{mix} + \alpha_{^3P_1}\mathcal{A}_{^3P_1}, \quad (39)$$

where α is the weight of each term given by

$$\alpha_x = \mathcal{A}_x/A_{hpf}(^1S_0, ^3P_0). \quad (40)$$

At first it seems the uncertainty of the $2s^2\ ^1S_0-2s2p\ ^3P_2$ hyperfine-induced electric dipole transition rate is more complicated to estimate, since the hyperfine mixing depends on both the nuclear magnetic dipole and the electric quadrupole hyperfine interaction. However, in the result section we showed that the electric quadrupole hyperfine interaction only gave a small contribution to the transition rate. To simplify our uncertainty estimate we therefore calculate the uncertainty of the $A^{M1}_{hpf}(^1S_0, ^3P_1)$ transition rate defined in Eq. (29) and assume that the relative size of the uncertainty is the same for the total hyperfine-induced transition rate. The expression for the $A^{M1}_{hpf}(^1S_0, ^3P_1)$ transition rate is similar to the one for the $A_{hpf}(^1S_0, ^1P_1)$ rate and the calculation of the uncertainty of the hyperfine-induced transition from $^3P_2$ is therefore done in the same way as outlined above.

The uncertainty of the energy-dependent terms of Eq. (38) were estimated by comparing our theoretical energies to the experimental ones taken from the NIST Atomic Spectra Database (version 3.1.5) [25]. The off-diagonal hyperfine interaction constants and the line strengths were estimated using the convergence method described above.

B. Results

Following the procedure outlined above, the uncertainty of the hyperfine-induced transitions and the two magnetic multipole transitions were estimated using both the quadratic and linear method. For each atomic parameter in the uncertainty expressions, a value of $\mathcal{K}$ was determined by studying the convergence. In cases where $\mathcal{K}$ had a value of less than 1, $\mathcal{K}$ was put to 1 to avoid underestimating the uncertainty.

The uncertainties of the $2s^2\ ^1S_0-2s2p\ ^3P_0$ hyperfine-induced transition rates, both using the quadratic and linear method, are presented in Table IV. In Table V only the linear uncertainty of the $2s^2\ ^1S_0-2s2p\ ^3P_2$ hyperfine-induced transition rate is presented, but the relative differences between the uncertainties using the two methods were the same for the $^3P_2$ quenching as for the $^3P_0$. Investigating the uncertainties along the isoelectronic sequence a similar pattern is found for both the hyperfine-induced transition rate from $^3P_0$ and $^3P_2$. $^{13}C^{2+}$ has the largest uncertainties. The uncertainties then decreases and are almost constant between $Z=11-16$, but then gradually increase going farther along the sequence. To understand these systematics we start by dividing the linear uncertainty into three different terms,

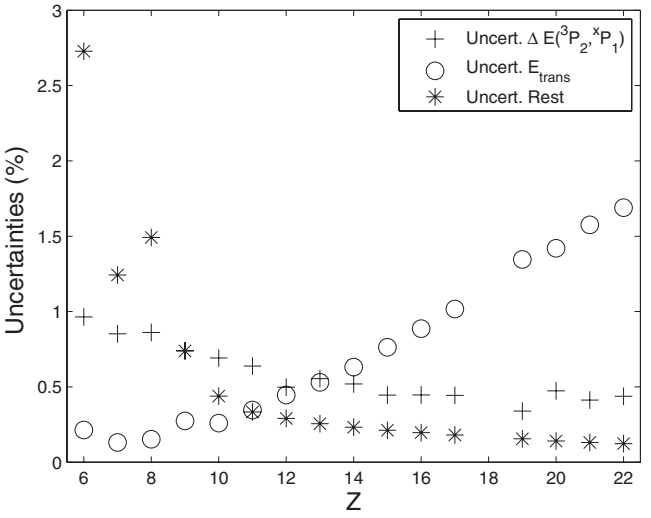

FIG. 7. The uncertainty of the hyperfine-induced transition from $2s2p\ ^3P_2$ divided into different terms (see text).

$$\delta A = \delta\Delta E + \delta E_{trans} + \delta Rest. \quad (41)$$

$\delta\Delta E$ are the uncertainties due to the errors in the energy splittings between the quenched levels and $^3P_1$ and $^1P_1$ respectively, δE_{trans} is the error due to the error in transition energy and $\delta Rest$ are the uncertainty contributions from the off-diagonal hyperfine interaction constants and the line strengths.

In Fig. 7 we have divided the uncertainty of the $^1S_0-^3P_2$ hyperfine induced transition into these three terms and plotted their uncertainty contributions along the isoelectronic sequence. From this plot it is found that the δE_{trans} term is the minor source of uncertainty in the beginning of the sequence. The size of this term gradually increases and dominates at the high end of the sequence. This trend shows that our method of calculation for the Be-like ions was better in predicting the excitation energies for the lower Z ions.

Turning to $\delta\Delta E$, it is found that this term gives a relatively small uncertainty contribution all along the sequence. There is a tendency for this term to slightly decrease going to the higher end of the sequence. This shows that our method of calculation was good in predicting the energy splittings among the excited levels all along the sequence.

The uncertainty contribution from $\delta Rest$ is the dominating source of uncertainty in the beginning of the sequence. The size of this term decreases going towards higher Z and finally it becomes of minor importance. $\delta Rest$ can be divided into a part depending on the off-diagonal hyperfine interaction constants and the line strengths. Without making a detailed study, the $\delta Rest$ term is dominated by the uncertainties in the line strengths. This can be understood through investigating the uncertainties in the four relevant atomic parameters. In

doing that it is found that the uncertainty of the $S_{^3P_1}$ line strength decrease from 5.8% in C^{2+} to 1.2% in Ti^{18+}, at the same time the uncertainty in $S_{^1P_1}$ decreases from 1.2% to 0.06%, while the uncertainty in the hypefine interaction constants drops from about 0.2% to 0.02%.

The differences between the linear and the quadratic error are smallest when there is one dominating source of uncertainty. For both quenching of the $^3P_0$ and the $^3P_2$ hyperfine levels the quadratic error approaches the linear error towards the end of the sequence. As mentioned above, the basis of the quadratic error is that the individual errors are independent of each other. This is not obvious in our case, and since we think it is better to over than under estimate the errors we decided to use only the linear errors for the $^3P_2$ level.

VII. CONCLUSIONS

It has been shown that the $2s2p\ ^3P_2$ level in Be-like ions are sensitive to hyperfine quenching in the lower end of the isoelectronic sequence. The hyperfine quenching not only affects the lifetime but can also manifest itself as spectral intensity redistribution through (a) changing branching ratios and (b) depleting metastable levels. The hyperfine induced transition channels have slightly higher Z dependencies than the $M2$ transition to the ground state. All along the sequence there are hyperfine levels where the hyperfine-induced transition is the dominant decay channel to the ground state. The $^3P_1-^3P_2$ $M1$ transition has a much stronger Z dependence than the hyperfine-induced transition. It was shown that the sensitivity to the hyperfine interaction decreases rather quickly after $Z=12$ where the $M1$ transition rate becomes higher than the $M2$ rate.

The transitions from $2s2p\ ^3P$ to the ground state plays an important role in diagnostics (Dufton and Kingston [36]) especially for low-density plasmas, e.g., planetary nebulas. Our results therefore call in question some of these type of calculations. We are working on the analysis of the most important cases [37].

The calculated rates for the hyperfine induced $2s^2\ ^1S_0-2s2p\ ^3P_0$ transition presented here are in agreement with the predicted rates from Cheng *et al.* [3] all along the isoelectronic sequence investigated here. Thus the discrepancies between the experimental determined hyperfine-induced transition rate for $^{47}Ti^{18+}$ by Schippers *et al.* [4] and the calculated rate remains.

ACKNOWLEDGMENT

This work was supported by the National Natural Science Foundation of China under Grant No. 10434050 and China Postdoctoral Science Foundation. This work was also partly supported by Shanghai Leading Academic Discipline Project, Project No. B107, Kungliga Fysiografiska Sällskapet i Lund, and the Swedish Research Council (Vetenskapsrådet).

[1] J. P. Marques, F. Parente, and P. Indelicato, Phys. Rev. A **47**, 929 (1993).
[2] T. Brage, P. G. Judge, A. Aboussaïd, M. R. Godefroid, P. Jönsson, A. Ynnerman, C. Froese Fischer, and D. S. Leckrone, Astrophys. J. **500**, 507 (1998).
[3] K. T. Cheng, M. H. Chen, and W. R. Johnson, Phys. Rev. A **77**, 052504 (2008).
[4] S. Schippers, E. W. Schmidt, D. Bernhardt, D. Yu, A. Muller, M. Lestinsky, D. A. Orlov, M. Grieser, R. Repnow, and A. Wolf, Phys. Rev. Lett. **98**, 033001 (2007).
[5] T. Brage, P. G. Judge, and C. R. Proffitt, Phys. Rev. Lett. **89**, 281101 (2002).
[6] K. Yao, M. Andersson, T. Brage, R. Hutton, P. Jönsson, and Y. Zou, Phys. Rev. Lett. **97**, 183001 (2006).
[7] K. Yao, M. Andersson, T. Brage, R. Hutton, P. Jönsson, and Y. Zou, Phys. Rev. Lett. **98**, 269903(E) (2007).
[8] E. Träbert, P. Beiersdorfer, G. V. Brown, K. Boyce, R. L. Kelley, C. A. Kilbourne, F. S. Porter, and A. Szymkowiak, Phys. Rev. A **73**, 022508 (2006).
[9] E. Träbert, P. Beiersdorfer, and G. V. Brown, Phys. Rev. Lett. **98**, 263001 (2007).
[10] M. Andersson, K. Yao, R. Hutton, Y. Zou, C. Y. Chen, and T. Brage, Phys. Rev. A **77**, 042509 (2008).
[11] R. H. Garstang, J. Opt. Soc. Am. **52**, 845 (1962).
[12] R. H. Garstang, Astrophys. J. **148**, 579 (1967).
[13] S. G. Porsev and A. Derevianko, Phys. Rev. A **69**, 042506 (2004).
[14] M. Andersson, Y. Liu, C. Y. Chen, R. Hutton, Y. Zou, and T. Brage (to be published).
[15] D. M. Brink and G. R. Satchler, *Angular Momentum* (Clarendon Press, Oxford, 1993).
[16] R. L. Kurucz, Phys. Scr., T **T47**, 110 (1993).
[17] I. P. Grant, *Relativistic Quantum Theory of Atoms and Molecules: Theory and Computation*, Springer Series on Atomic, Optical and Plasma Physics (Springer, Berlin, 2007).
[18] P. Jönsson, X. He, C. Froese Fischer, and I. P. Grant, Comput. Phys. Commun. **177**, 597 (2007).
[19] B. J. McKenzie, I. P. Grant, and P. H. Norrington, Comput. Phys. Commun. **21**, 233 (1980).
[20] I. P. Grant, J. Phys. B **7**, 1458 (1974).
[21] J. Olsen, M. R. Godefroid, P. Jönsson, P. Å. Malmqvist, and C. F. Fischer, Phys. Rev. E **52**, 4499 (1995).
[22] B. O. Roos, P. R. Taylor, and P. E. M. Siegbahn, Chem. Phys. **48**, 157 (1980).
[23] J. Olsen, B. O. Roos, P. Jørgensen, and H. J. Aa. Jensen, J. Chem. Phys. **89**, 2185 (1988).
[24] T. Brage and C. Froese Fischer, Phys. Scr., T **T47**, 18 (1993).
[25] Y. Ralchenko, A. E. Kramida, J. Reader, and NIST ASD Team, NIST Atomic Spectra Database (version 3.1.5), available at http://physics.nist.govasd3 (2008, November 27) (National Institute of Standards and Technology, Gaithersburg, MD, 2008).
[26] N. Reistad, R. Hutton, A. E. Nilsson, and I. Martinson, Phys. Scr. **34**, 151 (1986).
[27] L. Engström, B. Denne, J. O. Ekberg, K. W. Jones, C. Jupén,

U. Litzén, W. T. Meng, A. Trigueiros, and I. Martinson, Phys. Scr. **24**, 551 (1981).
[28] X. Tordoir, E. Bíemont, H. P. Garnir, P. D. Dumont, and E. Träbert, Eur. Phys. J. D **6**, 1 (1999).
[29] E. Träbert and P. H. Heckmann, Phys. Scr. **22**, 489 (1980).
[30] N. Bhattacharya, B. Bapat, S. A. Rangwala, S. V. K. Kumar, and E. Krishnakumar, Eur. Phys. J. D **2**, 125 (1998).
[31] J. Doerfert, E. Träbert, A. Wolf, D. Schwalm, and O. Uwira, Phys. Rev. Lett. **78**, 4355 (1997).
[32] J. Doerfert, E. Träbert, and A. Wolf, Hyperfine Interact. **99**, 155 (1996).
[33] E. Träbert, E. J. Knystautas, G. Saathoff, and A. Wolf, J. Phys. B **38**, 2395 (2005).
[34] A. Ynnerman and C. F. Fischer, Phys. Rev. A **51**, 2020 (1995).
[35] D. G. Ellis, Phys. Scr. **40**, 12 (1989).
[36] P. L. Dufton and A. E. Kingston, Adv. At. Mol. Phys. **17**, 355 (1981).
[37] M. Andersson, R. Hutton, Y. Zou, and T. Brage (unpublished).